KINEMATIC ANALYSIS AND TRAJECTORY PLANNING OF A TWO-LINK SCARA ROBOT

PATRIK SARGA[1], INGRID DELYOVA[1], DARINA HRONCOVA[1]

[1]Technical University of Kosice, Faculty of Mechanical Engineering, Kosice, Slovak Republic

DOI: 10.17973/MMSJ.2025_10_2024103

patrik.sarga@tuke.sk

This paper presents a comprehensive kinematic analysis of a two-link SCARA-type manipulator, focusing on the trajectory planning of its end-effector along a circular path. Using the FANUC SR-3iA/U as a reference platform, both inverse and forward kinematics were analyzed, with MATLAB simulations performed to generate smooth motion profiles based on fifth-order polynomial interpolation. The results demonstrate the manipulator's capability to execute precise, continuous trajectories while operating within workspace constraints.

KEYWORDS

SCARA robot, two-link manipulator, computer simulation, Matlab, kinematics, inverse solution, forward solution, trajectory

1 INTRODUCTION

The current advancement of manufacturing technologies, coupled with the rapid onset of digitalization in industry, presents new challenges in the fields of technical sciences and engineering practice. Automation and robotics have become an integral part of modern manufacturing processes, with applications ranging from mechanical engineering and construction to agriculture, healthcare, and various service industries. In response to the demands for precision, reliability, and flexibility, the development of new robotic systems focuses on optimizing motion and expanding the manipulation capabilities of robots [Majidi 2018, Adekola 2024, Singh 2024, Won 2024].

Modern production lines across various industrial sectors heavily rely on industrial robots. In practice, SCARA (Selective Compliance Articulated Robot Arm) robots are frequently employed for their efficiency in assembly line operations. Robotic arms, mounted on fixed or mobile platforms, are used for a wide range of handling tasks [Omodei 2000, Li 2020, Ulrich 2016, Sun 2023, Coronel-Escamilla 2017].

From a kinematic perspective, industrial robots consist of interconnected rigid bodies forming different types of kinematic chains, most commonly open chains or closed loops. When two bodies in a kinematic chain are connected in a manner that constrains their relative motion, they form a kinematic pair, typically linked by a joint. In robotics, the most common types are translational (prismatic) and rotational (revolute) kinematic pairs [Bozek 2014, Carbone 2016, Lee 2018, Alam 2023, Kim 1990].

Prismatic pairs enable linear motion, ideal for tasks requiring precise positioning. Revolute pairs, by contrast, allow rotational movement around a defined axis and are essential for operations requiring complex and dexterous motions, such as those in multi-axis robots used in machining or assembly.

Kinematic problems can be addressed using analytical, geometric, or experimental methods. Analytical approaches typically involve mathematical equations and transformations to describe manipulator motion. Forward kinematics is generally straightforward, whereas inverse kinematics can be computationally more challenging. Geometric methods, such as line transformations, provide alternative perspectives that may simplify analysis. Experimental methods bridge the gap between theoretical modeling and real-world applications [Hroncova 2012, 2023, 2024, Karupusamy 2024, Ju 2014, Kucuk 2006].

With the development of computer technology, experimental methods have become closely integrated with computational tools, enabling direct measurement of motion parameters during operation and improving measurement accuracy. Matrix methods in kinematics, due to their compact and intuitive representation, are highly suited for computational implementation and are now widely used [Fu 2013, Duleba 2013, Doriot 2004, Daya 2010].

In the following sections, we present a computational model and determine the trajectory of a robot's end effector during motion. The analysis begins with the inverse kinematics problem, followed by forward kinematics. The study introduces a methodology for kinematic analysis of a two-link robotic arm mounted on an upper fixed base. Both links are connected via revolute joints and perform rotational motion. The primary focus is to investigate the motion of the manipulator's end effector along a circular trajectory, deriving the profiles of angular variables in the joints and the corresponding time-dependent trajectory of the end effector, along with other kinematic relationships.

2 ANALYZED SCARA ROBOT

The objective is to analyze the motion of a robot end effector following a circular trajectory, using the ceiling-mounted FANUC SR-3iA/U (Fig. 1) robot as the experimental platform.

The FANUC SR-3iA/U robot is designed for high-speed and precise positioning, eliminating the "dead zone" typical of conventional SCARA robots. Its unique construction allows full utilization of the workspace beneath the arm and optimal distribution of the working area. Designed for cost-effectiveness and ease of configuration, it serves as a practical alternative to more expensive delta robots, making it suitable for a wide range of assembly, packaging, and material-handling tasks. With a pressing force of up to 150 N and very high operational speeds, it excels in pick-and-place applications, demonstrating versatility and productivity across diverse operating environments [Fanuc 2025].

The analysis of end-effector motion for the FANUC SR-3iA/U in a circular path requires consideration of multiple methodological and design aspects supported by the current state of research. FANUC robots, known for their precision and efficiency, can benefit from dynamic pose correction algorithms based on real-time feedback, enhancing the accuracy of the end-effector position. Experiments with FANUC robots have demonstrated position accuracy of ±0.050 mm and orientation accuracy of ±0.050°, which is crucial for consistent performance in complex trajectories, including circular motion [Gharaaty 2018].

In industrial applications where predefined path tracking is required, time-optimal motion control is often essential. This involves advanced higher-order inverse kinematics methods and resolving kinematic redundancy to achieve time-optimal motion along a specified trajectory. In this context, the FANUC SR-3iA/U can benefit from modern path-planning algorithms that consider its specific mechanical and control characteristics [Reiter 2018].

Motion planning strategies such as the manipulability-based optimal rapidly-exploring random tree (RRT) method are effective in enabling efficient trajectory tracking while avoiding singularities and optimizing joint configurations. This ensures

that the robot operates within its motion constraints while maintaining high manipulability of the end effector throughout the operation [Shen 2023].

When programming the robot for circular motion, the selection and tuning of waypoints and speed settings play a critical role. Smooth blending between motion primitives, such as Cartesian linear and circular segments, must be optimized to minimize tracking errors, especially near singularities or in extreme arm postures. A systematic approach involving careful waypoint selection and adjustment of motion primitives enhances both tracking accuracy and speed uniformity [He 2024, Jia 2024].

In summary, the FANUC SR-3iA/U can efficiently execute circular end-effector tasks by employing dynamic pose correction, advanced inverse kinematics, and sophisticated path-planning algorithms. These methods, supported by contemporary research, provide a solid foundation for robust motion control and optimization in industrial environments.

Figure 1. FANUC SR-3*i*A/U [Fanuc 2025]

The kinematic scheme represents a SCARA-type robot consisting of two revolute joints and a terminal link performing translational motion (Fig. 2). The rotation angle of the first arm is denoted as θ_1, the rotation angle of the second arm as θ_2, and the translational displacement of the terminal link as d_3.

The manipulator model in Fig. 2 illustrates the range of motion of the end effector during robot operation.

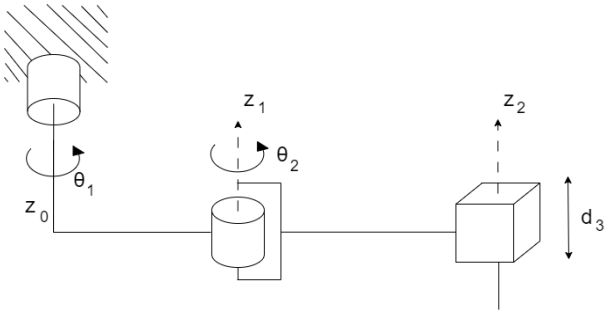

Figure 2. A two-link robotic arm of SCARA on an upper fixed base

The subsequent section addresses the inverse and forward kinematics of the two arms shown in Fig. 2. Trajectories of the end effector between selected workspace points will be determined, the workspace will be visualized, and the profiles of angular variables at the manipulator joints will be obtained.

3 THE INVERSE KINEMATICS

We analyze a two-link robotic arm with link lengths $L_1 = 0.4$ m and $L_2 = 0.3$ m. The arm is fixed on an overhead base. Revolute joints are located at points O_1 and O_2, with rotation angles θ_1 and θ_2 for the first and second arms, respectively. The generalized coordinates of the two-link arm (Fig. 2) are q_1 and q_2, where $q_1 = \theta_1$ and $q_2 = \theta_2$.

The forward kinematic equations determining the position of the end point $P[x_P,y_P]$ given known θ_1 and θ_2 are:

$$x_P = L_1\cos\theta_1 + L_2\cos(\theta_1 + \theta_2) \quad (1)$$

$$y_P = L_1\sin\theta_1 + L_2\sin(\theta_1 + \theta_2) \quad (2)$$

The motion of point P is analyzed for the base coordinate system O_0,x_0,y_0,z_0. Link 1, with coordinate system O_1,x_1,y_1,z_1, rotates with angle θ_1 around axis $z_0 \equiv z_1$, where $\theta_1 = \theta_1(t)$. Link 2 rotates with angle θ_2 around axis $O_2 \equiv z_2$, where $\theta_2 = \theta_2(t)$.

In inverse kinematics, we proceed oppositely compared to forward kinematics: from a known position of $P[x_P,y_P]$, we determine θ_1 and θ_2 using Eqs. (1) – (2). This problem generally has multiple solutions, a common challenge in robotics. θ_1 represents the rotation of the first arm relative to the base, while θ_2 represents the rotation of the second arm relative to the first. We will compute the arm angles at the initial position of point P_0 given the coordinates x_{P0} and y_{P0} at time t=0, yielding values for θ_{10} and θ_{20}. Next, at the final position of point P_{1tfin} with coordinates x_{P1tfin} and y_{P1tfin} at time $t=t_{fin}$, we will determine the corresponding angles θ_{1tfin} and θ_{2tfin}. Calculations are performed for a circular path between points A–H (Fig. 3), with coordinates listed in Tables 1–2. Points J and K represent maximum reach.

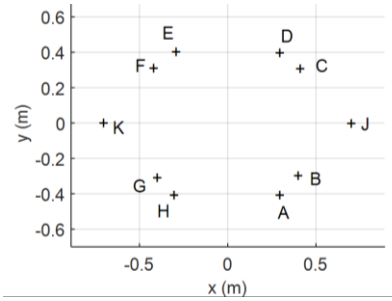

Figure 3. The positions A, B, C, D, E, F, G, H, J, K within the workspace

Table 1. Coordinates x_i, y_i of the points A, B, C, D, E

	A	B	C	D	E
x_i [m]	0.3	0.4	0.4	0.3	-0.3
y_i [m]	-0.4	-0.3	0.3	0.4	0.4

Table 2. Coordinates x_i, y_i of the points F, G, H, J, K

	F	G	H	J	K
x_i [m]	-0.4	-0.4	-0.3	0.7	-0.7
y_i [m]	0.3	-0.3	-0.4	0.0	0.0

By solving Eqs. (1) – (2) for the initial and final positions, the joint angles at each position are determined (Tables 3 and 4).

Table 3. Angles when the endpoint moves between points A-B, B-C, C-D, D-E

	A-B	B-C	C-D	D-E
θ_{10}	-90°	-73.74°	-73.74°	90°
θ_{20}	90°	90°	-90°	-90°
θ_{1tfin}	-73.74°	0°	90°	163.74°
θ_{2tfin}	90°	90°	-90°	-90°

Table 4. Angles when the endpoint moves between points E-F, F-G, H-A, and J-K

	E-F	F-G	G-H	H-A	J-K
θ_{10}	163.74°	106.26°	-106.26°	-90°	0°
θ_{20}	-90°	90°	-90°	-90°	0°
θ_{1tfi}	180°	180°	-90°	-16.26°	180°
θ_{2tfi}	-90°	90°	-90°	-90°	0°

The paths along which the end point will move between the specified points will be determined by solving the forward kinematics problem in the next section.

4 THE FORWARD KINEMATICS

To ensure smooth motion with continuous position, velocity, and acceleration profiles, the end-effector trajectory is generated using fifth-order polynomial interpolation for each joint. The angular displacement of Link 1 is given by:

$$\theta_1(t) = a_1t^5 + a_2t^4 + a_3t^3 + a_4t^2 + a_5t + a_6 \quad (3)$$

Similarly, the angular displacement of Link 2 is expressed as:

$$\theta_2(t) = b_1t^5 + b_2t^4 + b_3t^3 + b_4t^2 + b_5t + b_6 \quad (4)$$

The coefficients a_i and b_i (i=1,…,6) are computed from the boundary conditions of the motion.

For the circular motion case analyzed here, the second link maintains a constant relative angle to the first link, resulting in zero coefficients in equation (4). Thus, only the coefficients a_1,a_2,a_3 for equation (3) are non-zero, as listed in Tables 5–7.

Table 5. The coefficients a_1, a_2, a_3 of the polynomial (3) of points A-E

	A-B	B-C	C-D	D-E
a_1	0.0532	0.2413	0.0532	0.2413
a_2	-0.2661	-1.2066	0.2661	-1.2066
a_3	0.3547	1.6088	0.3547	1.6088

Table 6. The coefficients a_1, a_2, a_3 of the polynomial (3) of points E-H

	E-F	F-G	G-H
a_1	0.0532	0.2413	0.0532
a_2	0.2661	1.2066	0.2661
a_3	0.3547	1.6088	0.3547

Table 7. The coefficients a_1, a_2, a_3 of the polynomial (3) of points H-K

	H-A	J-K
a_1	0.2413	0.5890
a_2	1.2066	-2.9452
a_3	1.6088	3.9270

Subsequently, we derive the trajectory profile for the angular values from Table 3 and Table 4 as the end point moves through the individual points whose coordinates are given in Table 1 and Table 2. The feasibility of this motion needs to be evaluated within the workspace of the two-link manipulator. The workspace of the end point for arms with lengths L_1 and L_2, given the joint angle constraints $0° \le \theta_1 \le 360°$ and $0° \le \theta_2 \le 180°$, is illustrated in the following figures. The plots of the individual trajectories $y_i = f(x_i)$, where i = 1,2,…,9, showing the transition of the end point from A to B, then B–C, C–D, D–E, E–F, F–G, G–H, H–A, and J–K, are presented in Fig. 4.

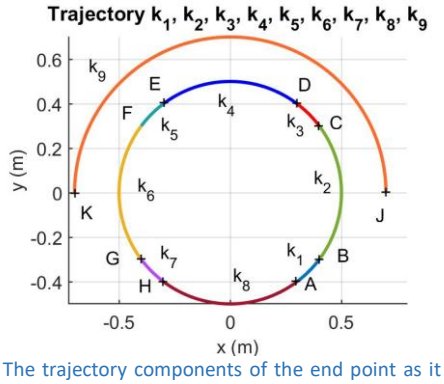

Figure 4. The trajectory components of the end point as it transitions from the initial position at point A to the final position at point B, and subsequently from point B to point C, C-D, D-E, E-F, F-G, G-H, H-A, and J-K

The trajectory generation must comply with the manipulator's workspace constraints: $0° \le \theta_1 \le 360°$ and $0° \le \theta_2 \le 180°$ (Fig.5).

The complete workspace is segmented into operational zones based on θ_2 intervals:

- p: $0° \le \theta_2 \le 30°$
- q: $30° \le \theta_2 \le 60°$
- r: $60° \le \theta_2 \le 90°$
- s: $90° \le \theta_2 \le 120°$
- u: $120° \le \theta_2 \le 150°$
- w: $150° \le \theta_2 \le 180°$

This zoning allows for a better understanding of reachable positions and facilitates optimized waypoint placement during trajectory planning.

The end-effector follows a predefined closed path, passing sequentially through points A–B, B–C, C–D, D–E, E–F, F–G, G–H, H–A, and J–K. The coordinates of these points (given in Tables 1 and 2) serve as input for solving the inverse kinematics problem, yielding the joint angles required for each segment. These joint angles are then used as the start and end conditions for the fifth-order polynomials, ensuring smooth transitions between segments.

The generated polynomial coefficients define not only the positional path but also the velocity and acceleration profiles of each joint, ensuring jerk minimization—a crucial factor in reducing wear, improving accuracy, and maintaining stability in high-speed industrial operations.

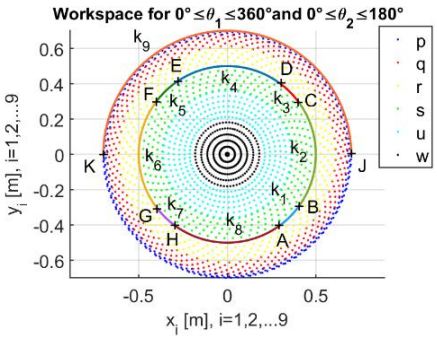

Figure 5. Coordinate pairs (x, y) are plotted for various combinations of θ_1 (0° to 360°) and θ_2 (0° to 180°)

The graphical representation of kinematic parameters obtained by this method will be presented in the following sections of the paper.

5 GRAPHICAL REPRESENTATION OF KINEMATIC PARAMETERS

The kinematic behavior of the two-link SCARA manipulator was evaluated exclusively for the first link, as the second link maintained a fixed relative position throughout the motion. Consequently, only the angular displacement $\theta_1(t)$, angular velocity $\omega_1(t)$, and angular acceleration $\alpha_1(t)$ of the first link were analyzed. The results, obtained from MATLAB simulations, were evaluated over time for each segment of motion between predefined points along the end-effector's trajectory. The simulated motion sequences included A–B, B–C, C–D, D–E, E–F, F–G, G–H, and H–A.

For each trajectory segment, $\theta_1(t)$ was computed using the fifth-order polynomial interpolation described in Eq. (3), ensuring smooth transitions in position, velocity, and acceleration between waypoints. The resulting plots (Fig. 6) illustrate the continuous evolution of θ_1 during motion, showing how the Link 1 angle changes as the end-effector moves along different parts of the circular path.

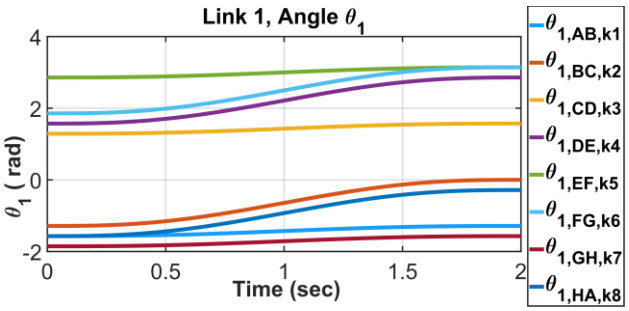

Figure 6. The rotation angles θ_1 of Link 1 (arm 1) as the endpoint transitions from the initial point A to the final point B (A-B), continuing through B-C, C-D, D-E, E-F, F-G, G-H, H-A

The angular velocity profiles $\omega_1(t)$ (Fig. 7) provide insight into the dynamic response of Link 1. The fifth-order polynomial interpolation ensures zero initial and final velocities for each segment, preventing abrupt speed changes that could lead to mechanical stress or vibration. The velocity curves highlight regions of peak motion demand, which are particularly important for evaluating motor sizing, drive selection, and control loop tuning.

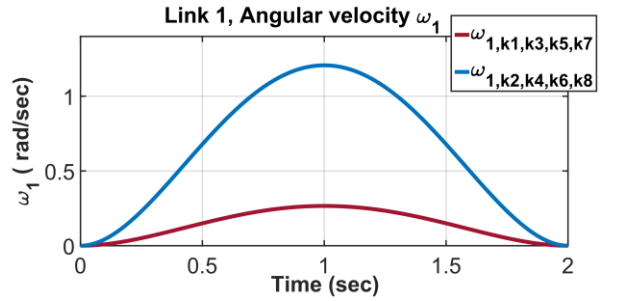

Figure 7. The angular velocity ω_1 of Link 1 (arm 1) as it transitions from the initial point A to the final point B (A-B), followed by B-C, C-D, D-E, E-F, F-G, G-H, H-A

Similarly, the angular acceleration profiles α1(t) of Link 1 are illustrated in Fig. 8.

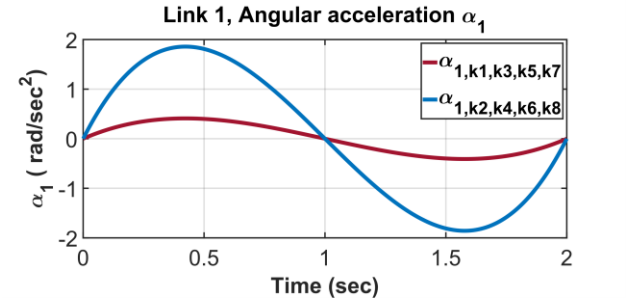

Figure 8. Angular accelerations α_1 when the endpoint is moving from the initial point A to the final point B (A-B), followed by B-C, C-D, D-E, E-F, F-G, G-H, H-A

Other dependencies between the kinematic quantities of Link 1 are shown in the following figures (Fig. 9, Fig. 10, Fig. 11).

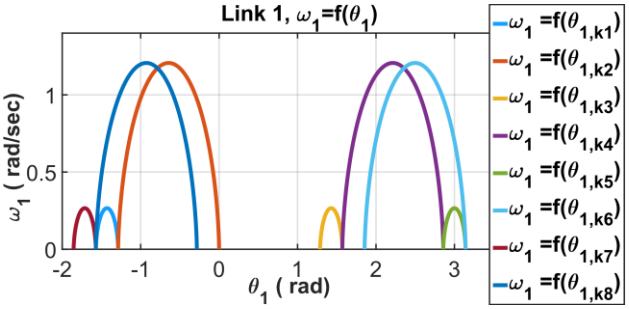

Figure 9. Angular velocity ω_1 dependent on the rotation angles θ_1 of Link 1 (arm 1)

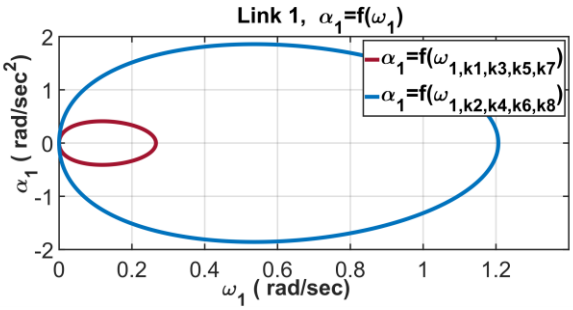

Figure 10. Angular acceleration α_1 dependent on the angular velocity ω_1 of Link 1 (arm 1)

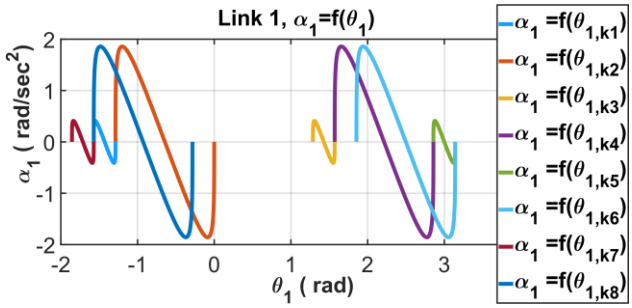

Figure 11. Angular acceleration α_1 dependent on the rotation angles θ_1 of Link 1 (arm 1)

In the next part, the trajectory k_9 (Fig. 9) is analyzed, which represents motion at the maximum reach of the manipulator arm. This configuration generates the largest moment arm and thus the most significant dynamic demands on the drive system. The corresponding θ_1 (Fig. 10), ω_1 (Fig. 11), and α_1 profiles (Fig. 12) show notably higher acceleration peaks compared to trajectories within the central workspace region, emphasizing the importance of workspace position in motion planning.

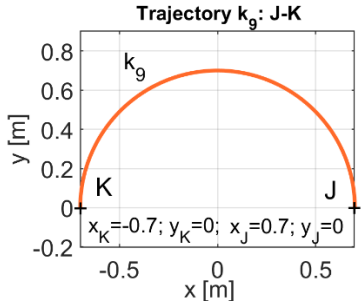

Figure 9. Trajectory k_9 at maximum extension

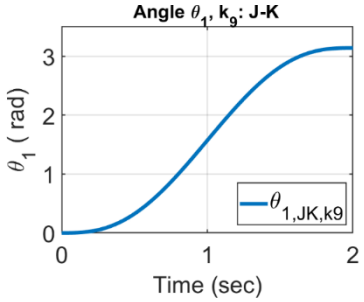

Figure 10. The rotation angle θ_1 at maximum extension

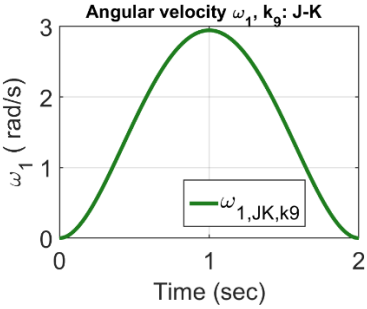

Figure 11. Angular velocity ω_1 at maximum extension

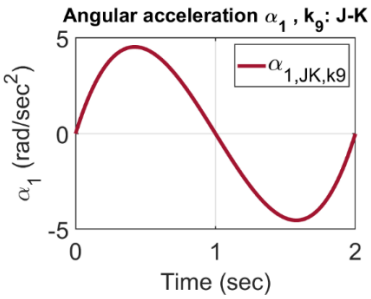

Figure 12. Angular acceleration α_1 at maximum extension.

The methodology demonstrated here — using MATLAB for simulation, polynomial trajectory generation, and graphical evaluation of kinematic variables — applies not only to circular motion but also to arbitrary end-effector paths. It offers a practical framework for both industrial optimization of motion planning and for educational use in teaching forward and inverse kinematics principles.

6 CONCLUSIONS

This study presented a detailed kinematic analysis and trajectory planning methodology for a two-link SCARA-type manipulator, using the FANUC SR-3iA/U as the experimental reference platform. Both inverse and forward kinematic models were derived, enabling the precise determination of joint angles required for predefined end-effector positions. The use of fifth-order polynomial interpolation provided smooth angular displacement, velocity, and acceleration profiles, ensuring continuous and vibration-free motion between target points.

Simulation results in MATLAB confirmed that the proposed method enables accurate end-effector motion along a circular path while respecting the mechanical and workspace constraints of the manipulator.

The presented approach applies not only to industrial applications requiring high-speed pick-and-place operations but also in educational environments for teaching forward and inverse kinematics. Future research will focus on integrating dynamic modeling, optimizing time-parameterized trajectories for energy efficiency, and validating the method through physical experiments on the FANUC SR-3iA/U platform.

ACKNOWLEDGMENTS

The authors would like to thank the Slovak Grant Agency project VEGA 1/0169/22 and grant project KEGA 039TUKE-4/2024 supported by the Ministry of Education of the Slovak Republic.

REFERENCES

[Adekola 2024] Adebayo, R.A., Olajiga, O.K., Festus-Ikhuoria, I.C., Obiuto, N.C. Robotics in Manufacturing: A Review of Advances in Automation and Workforce Implications. International Journal of Advanced Multidisciplinary Research and Studies, 2024, Vol. 4, No. 2, pp. 632-638. https://doi.org/10.62225/2583049x.2024.4.2.2549.

[Bozek 2014] Bozek, P., Turygin, Y. Measurement of the operating parameters and numerical analysis of the mechanical subsystem. Measurement Science Review, 2014, Vol. 14, No. 4, pp. 198-203.

[Carbone 2016] Carbone, G., Di Nuovo, A. A hybrid multi-objective approach for optimal path planning of a hexapod robot a preliminary study. Lecture Notes in Computer Science, 2016, Vol. 9668, pp. 131-144.

[Coronel-Escamilla 2017] Coronel-Escamilla, A., Torres, F., Gomez-Aguilar, J.F., et al. On the trajectory tracking control for an SCARA robot manipulator in a fractional model driven by induction motors with PSO tuning. Multibody System Dynamics, 2017, Vol. 43, No. 3, pp. 257-277. https://doi.org/10.1007/s11044-017-9586-3.

[Daya 2010] Daya, B., Akoum, M., Khawandi, S. Applying Neural Network Architecture for Inverse Kinematics Problem in Robotics. Journal of Software Engineering and Applications, 2010, Vol. 3, No. 3, pp. 230-239. https://doi.org/10.4236/jsea.2010.33028.

[Doriot 2004] Doriot, N., Cheze, L. A three-dimensional kinematic and dynamic study of the lower limb during the stance phase of gait using an homogeneous matrix approach. IEEE Transactions on Biomedical Engineering, 2004, Vol. 51, No. 1, pp. 21-27. https://doi.org/10.1109/tbme.2003.820357.

[Duleba 2013] Duleba, I., Opalka, M. A comparison of Jacobian-based methods of inverse kinematics for serial robot manipulators. International Journal of Applied Mathematics and Computer Science, 2013, Vol. 23, No. 2, pp. 373-382. https://doi.org/10.2478/amcs-2013-0028.

[FANUC 2025] FANUC Europe, SR-3iA/U SCARA robot, FANUC Europe Corporation, 2025. Available from: www.fanuc.eu/eu-en/product/robot/sr-3iau.

[Fu 2013] Fu, Z., Yang, W., Yang, Z. Solution of Inverse Kinematics for 6R Robot Manipulators With Offset Wrist Based on Geometric Algebra. Journal of Mechanisms and Robotics, 2013, Vol. 5, No. 3. https://doi.org/10.1115/1.4024239.

[Gharaaty 2018] Gharaaty, S., Shu, T., Xie, W.F., Joubair, A., Bonev, I.A., Online pose correction of an industrial robot using an optical coordinate measure machine system. International Journal of Advanced Robotic Systems, 2018, Vol. 15, No. 4. https://doi.org/10.1177/1729881418787915.

[He 2024] He, H., Saunders, G., Wason, J., et al. Fast and Accurate Relative Motion Tracking for Dual Industrial Robots. IEEE Robotics and Automation Letters, 2024, Vol. 9, No. 11, pp. 10153-10160. https://doi.org/10.1109/lra.2024.3471455.

[Hroncova 2012] Hroncova, D., Sarga, P., Gmiterko, A., Simulation of mechanical system with two degrees of freedom with Bond Graphs and Matlab/Simulink. Procedia Engineering, 2012, Vol. 48, pp. 223-232.

[Hroncova 2023] Hroncova, D., Sarga, P., Sincak, P.J., Merva, T., Brada, L. Inverse and forward kinematics and dynamics of a two link robot arm. MM Science Journal, 2023, No. December. DOI: 10.17973/MMSJ.2023_12_2023067.

[Hroncova 2024] Hroncova, D., Sarga, P., Prada, E. Exploration of the inverse and forward kinematics of a two-link robot arm using Matlab. MM Science Journal, 2024, No. June. DOI: 10.17973/MMSJ.2024_06_2024022.

[Jia 2024] Jia, X., Zhao, B., Liu, J., Zhang, S. A trajectory planning method for robotic arms based on improved dynamic motion primitives, Industrial Robot. International Journal of Robotics Research and Application, 2024, Vol. 51, No. 5. https://doi.org/10.1108/ir-12-2023-0322.

[Ju 2014] Ju, Z., Ma, H., Yang, C. Kinematics modeling and experimental verification of baxter robot, In: Proceedings of the 33rd Chinese Control Conference,

Nanjing, China, 2014, pp. 8518-8523. https://doi.org/10.1109/chicc.2014.6896430.

[Karupusamy 2024] Karupusamy, S., Maruthachalam, S., Veerasamy, B. Kinematic Modeling and Performance Analysis of a 5-DoF Robot for Welding Applications. Machines, 2024, Vol. 12, No. 6, 378. https://doi.org/10.3390/machines12060378.

[Kim 1990] Kim, J., Kumar, V.R., Kinematics of robot manipulators via line transformations. Journal of Robotic Systems, 1990, Vol. 7, No. 4, pp. 649-674. https://doi.org/10.1002/rob.4620070408.

[Kucuk 2006] Kucuk, S., Bingul, Z. Robot Kinematics: Forward and Inverse Kinematics. Pro Literatur Germany Ars Austria, 2006. https://doi.org/10.5772/5015.

[Lee 2018] Lee, J.-D., Li, W.-C., Shen, J.-H., Chuang, C.-W. Multi-robotic arms automated production line, In: 2018 4th Int. Conf. on Control, Automation and Robotics (ICCAR), Auckland, New Zealand, 2018, pp. 26-30. https://doi.org/10.1109/iccar.2018.8384639.

[Li 2020] Li, Z., Luo, X., Li, S. An overview of calibration technology of industrial robots. IEEE/CAA Journal of Automatica Sinica, 2020, Vol. 8, No. 1, pp. 23-36. https://doi.org/10.1109/jas.2020.1003381.

[Majidi 2018] Majidi, C. Soft-Matter Engineering for Soft Robotics. Advanced Materials Technologies, 2018, Vol. 4, No. 2, 1800477. https://doi.org/10.1002/admt.201800477.

[Omodei 2000] Omodei, A., Adamini, R., Legnani, G. Three methodologies for the calibration of industrial manipulators: Experimental results on a SCARA robot. Journal of Robotic Systems, 2000, Vol. 17, No. 6, pp. 291-307. https://doi.org/10.1002/(sici)1097-4563(200006)17:6<291::aid-rob1>3.0.co;2-u.

[Reiter 2018] Reiter, A., Muller, A., Gattringer, H. On Higher Order Inverse Kinematics Methods in Time-Optimal Trajectory Planning for Kinematically Redundant Manipulators. IEEE Transactions on Industrial Informatics, 2018, Vol. 14, No. 4, pp. 1681-1690. https://doi.org/10.1109/tii.2018.2792002.

[Shen 2023] Shen, H., Tang, J., Zhou, T., Xie, W.-F., Adaptive Manipulability-Based Path Planning Strategy for Industrial Robot Manipulators. IEEE/ASME Trans. on Mechatronics, 2023, Vol. 28, No. 3, pp. 1742-1753. https://doi.org/10.1109/tmech.2022.3231467.

[Singh 2024] Singh, M., Khan, S. Advances in Autonomous Robotics: Integrating AI and Machine Learning for Enhanced Automation and Control in Industrial Applications. Int. Journal for Multidimensional Research Perspectives, 2024, Vol. 2, No. 4, pp. 74-90. https://doi.org/10.61877/ijmrp.v2i4.135.

[Sun 2023] Sun, X., Terada, H., Ishida, K., Shibayama, K., Makino, K. Development of the "Quad-SCARA" platform and its collision avoidance based on Buffered Voronoi Cell. Robotica, 2023, Vol. 41, No. 12, pp. 3687-3701. https://doi.org/10.1017/s0263574723001236.

[Ulrich 2016] Ulrich, M., Steger, C. Hand-eye calibration of SCARA robots using dual quaternions. Pattern Recognition and Image Analysis, 2016, Vol. 26, No. 1, pp. 231-239, doi.org/10.1134/s1054661816010272.

[Won 2020] Won, P., Cho, H., Shin, J., et al. Transparent Soft Actuators/Sensors and Camouflage Skins for Imperceptible Soft Robotics. Advanced Materials, 2020, Vol. 33, No. 19, 2002397. https://doi.org/10.1002/adma.202002397.

CONTACTS:

Patrik Sarga, Assoc. Prof., Ing., PhD.
Technical University of Kosice, Faculty of Mechanical Engineering
Institute of Automation, Mechatronics, Robotics and Production Techniques
Letna 9, 04200 Kosice, Slovak Republic
patrik.sarga@tuke.sk